GCM SIMULATIONS OF APHELION SEASON TROPICAL CLOUD AND TEMPERATURE STRUCTURE

R. J. Wilson, *Geophysical Fluid Dynamics Laboratory, Princeton, NJ (John.Wilson@noaa.gov)*, **E. Millour, T. Navarro, F. Forget**, *Laboratoire de Météorologie Dynamique, Paris France*, **M. Kahre**, *NASA Ames Research Center, Moffett Field CA, USA.*

Introduction:

There is a growing appreciation that the radiative effects of water ice clouds may play a significant role in shaping atmospheric temperature structure. *Wilson et al*. [2008] used the UK Reanalysis to identify a cold bias in zonal mean temperature in Mars Global Climate Model (MGCM) simulations of tropical temperature that robustly develops in the NH summer solstice season. They further showed that radiatively active clouds (RAC) can plausibly account for the latitude-height distribution of the cold bias. More recently, inclusion of radiatively active water ice clouds has been found to yield improved agreement with spacecraft observations [*Haberle et al*. 2011; *Wilson*, 2011b; *Madeleine et al*. 2012]. The evidence for coupling between tropical clouds and the thermal tide first seen in MGS Radio Science observations [*Hinson and Wilson*, 2004] has been reinforced by the much more extensive and comprehensive data returned from Mars Climate Sounder (MCS) [*Wilson*, 2011; *Wilson and Guzewich*, submitted paper]. In this presentation we consider the results from several MGCMs in order to survey the range of cloud and temperature distributions being simulated with current cloud parameterizations. We will present results from models developed by the LMD, Ames, and GFDL modeling teams and propose and assess diagnostic measures of cloud influence for comparison with MCS data.

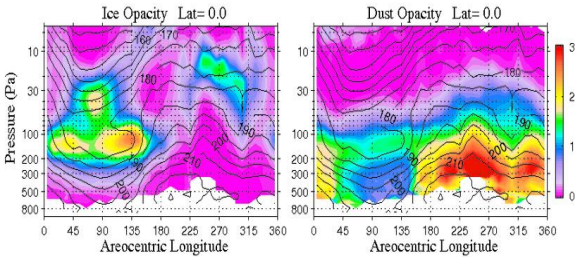

Figure 1. (a) Seasonal evolution of zonally-averaged equatorial water ice cloud opacity (shading) and temperature (contours) derived from 0300 local time MCS retrievals from MY30 and 31. Opacity units are 10^{-3} km^{-1}. Temperature is contoured in 10 K intervals. (b) Zonally-averaged nighttime dust opacity.

Aspects of the LMD cloud simulation are described by *Madeleine et al*. [2012] and *Pottier et al*. [2014]. LMD results have also been made publically available in the form of the Mars Climate Database (MCD) [*Millour et al*. 2014], and we make use of results from versions 4.2 (dust only) and 5.1 (RAC). Ames model cloud simulations are described in *Haberle et al*. [2011] and *Kahre et al*. [2014]. GFDL model simulations with RAC are described in *Greybush et al*. [2012], and *Kleinbohl et al*. [2013].

MCS Observations and GCM Simulations:

The seasonal evolution of the nighttime zonal mean equatorial aerosol and temperatures fields is summarized in Figure 1. The aphelion season equatorial cloud belt is particularly prominent and abruptly dissipates after L_s ~ 160° when zonal mean temperatures rapidly increase. This timing is coincident with an increase in dust opacity. The vertical distribution of the tropical dust opacity has a well-defined maximum between 100-200 Pa during the L_s = 40-135° season that is correlated to the ice cloud opacity. This tropical dust maximum has been identified by *Heavens et al*. [2011] and *Guzewich et al*. [2013] and it motivates the study of a possible coupling of the dust and cloud fields. It can be seen that the aphelion season clouds are associated with a more isothermal temperature structure within the 200-40 Pa layer of atmosphere. TES profiling lacked the resolution to identify this vertical variation in lapse rate, which has been interpreted as a manifestation of cloud influence [*Wilson and Guzewich*, submitted paper].

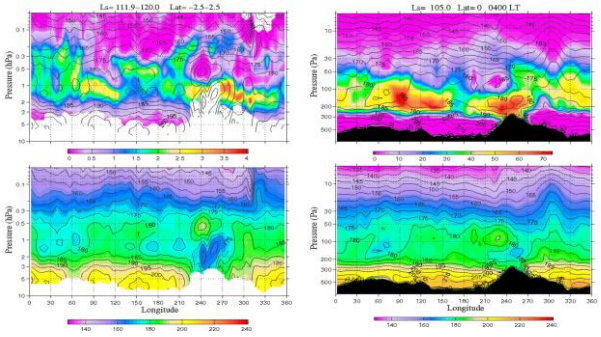

Figure 2 (Left column) Longitude-pressure distribution of nighttime (0300 LT) equatorial water ice cloud opacity (top) and temperature (bottom) derived from MCS retrievals from MY30 for L_s = 112-120°. Opacity units are $10^{-3}$$km^{-1}$. Temperature is contoured in 5 K intervals. (Right column) Cloud mixing ratio (ppm, top) and temperature (bottom) from a GFDL MGCM simulation with RAC.

Figure 2 shows a longitude section of equatorial temperature and cloud opacity as observed by MCS during the summer solstice season. Data from MY30

are shown, but the structures are essentially identical to those for MY29 and MY31. The presence of the strong cold nighttime temperature anomaly in the Tharsis region is evidently a robust feature of the equatorial atmosphere during the L_s=20-130° season, with little difference seen between the three Mars years examined (MY 29-31). Also shown are results from a GFDL MGCM simulation, which captures the main features of the observed structure. Figure 3 illustrates the impact of RAC using the LMD MCD version 4.2 simulation without water ice clouds and the MCD 5.1 simulation with water ice clouds. The lapse rate is much more uniform from the surface to 20 Pa in the dust-only simulation and there is relatively little zonal modulation of temperature. The effect of clouds is consistent between the two models with RAC in figures 2 and 3. There are differences in the zonal distribution of clouds, which may reflect differences in simulated particle sizes and sedimentation. For example, GFDL model simulations indicate that larger particles result in faster sedimentation that yields shallower clouds with greater longitudinal isolation. It should be noted that Figure 2 shows MCS cloud opacity, rather than density-scaled opacity, which is roughly proportional to mixing ratio. Consequently, the simulated cloud fields are notably less deep than implied by the observations, a discrepancy that was noted by *Heavens et al*. [2010].

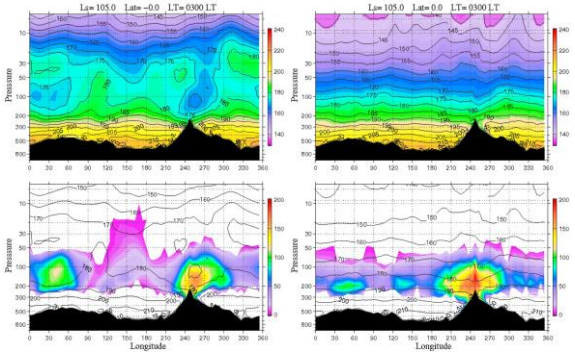

Figure 3 Longitude-pressure distribution of equatorial nighttime temperature (top) and cloud mixing ratio (bottom) for LMD simulations with (left column; MCD V5.1) and without (right column; MCD V4.2) radiatively active water ice clouds

The daytime aphelion season tropical cloud belt appears to be centered at ~30 Pa, but high opacity severely limits the ability to successfully retrieve temperature and aerosol profiles from MCS radiances and properly characterize the afternoon cloud and temperature structure. Therefore we rely on simulations to extrapolate to other local times to gain insight into the role of clouds in shaping the diurnal variation of temperature. Figure 4 shows the diurnal variation of zonally-averaged equatorial temperature and related fields from a simulation employing RAC. Clouds contribute significantly to the radiative forcing of the atmosphere, as shown in Figure 4d. The simulated diurnal mean heating rate is ~10-15 K [*Kleinböhl et al*. [2013]. The dominant contribution in the tropics is a strong radiative heating by the absorption of upwelling IR radiation from the relatively hot daytime surface.

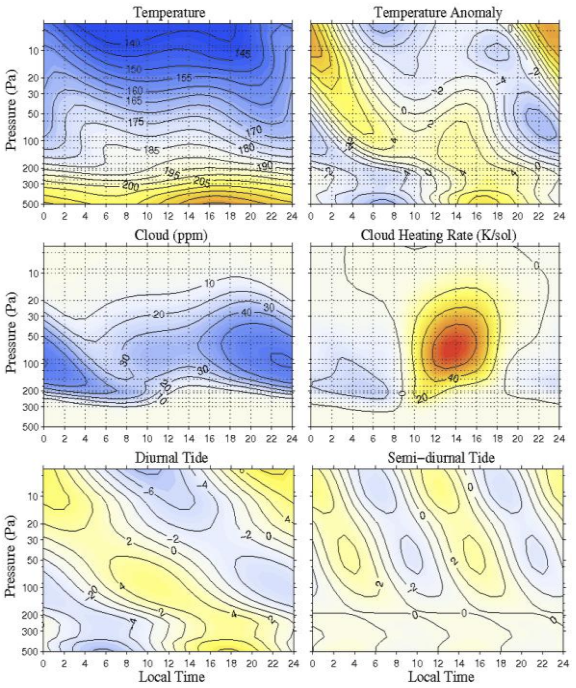

Figure 4. (a) Diurnal variation of zonally-averaged equatorial temperature from a GFDL MGCM simulation with RAC. (b) The diurnally varying component of the temperature field. (c) As for (a) but for cloud water ice. (d) The diurnal variation of the LW heating (K/sol) due to the presence of water ice clouds. (e) The diurnal harmonic, S_1, of the temperature anomaly. (f) The semi-diurnal tide S_2.

Clouds also contribute to enhanced nighttime cooling by LW emission to space. The enhanced downward IR radiation by clouds also influences surface temperature, as discussed in the following section. The sun-synchronous (migrating) diurnal and semi-diurnal tides are also shown. The diurnal tide (S_1) has the character of a vertically propagating gravity wave with a vertical wavelength of ~35 km, while that of the semi-diurnal tide (S_2) is much longer. As has been noted in previous studies [*Hinson and Wilson*, 2004; *Lee et al*. 2009], the cloud diurnal variation is shaped by the temperature structure, with the center of cloud mass descending downward in phase with the diurnal tide. The relatively stable nighttime atmosphere between 200 and 50 Pa is a consequence of the vertically propagating diurnal tide, the dominant atmospheric response to the diurnal variation of thermal forcing. Nighttime vertical velocities (not shown) are downward between 20-100 Pa, resulting in strong adiabatic warming above the simulated cloud deck and contributing to atmos-

pheric stability in this layer. The considerable longitudinal variability in Figures 2 and 3 is evidence for significant non-migrating (non-sun-synchronous) tide excitation. As discussed in *Hinson and Wilson* [2004] and *Wilson and Guzewich* [submitted paper, 2013], this zonal modulation of the tide is influenced by topography and localized cloud IR emission, with the cloud forcing enhancing the tide response. The temperature inversion over Tharsis is the result of locally enhanced tide forcing. Simulation suggests a low-level cooling rate of ~40 K/sol in the Tharsis region [*Wilson and Guzewich* [submitted paper, 2013] during the early morning hours.

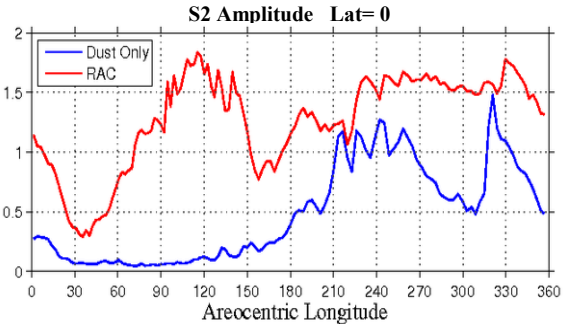

Figure 5. The seasonally varying amplitude of the semi-diurnal component of equatorial T_{15} for LMD simulations with and without radiatively active clouds. The dust scenario is for MY26

Assessing Cloud Forcing:

It is noteworthy that the simulated daytime cloud heating rate in Figure 4d is 2-3 times larger than estimated by *Steele et al.* [2014, Figure 4]. This is likely due to the thicker clouds in typical simulations. This difference highlights the need for a means of assessing cloud impact. Here we describe two approaches. By virtue of the long vertical wavelength and broad meridional structure of the dominant semi-diurnal Hough mode, the migrating semi-diurnal surface pressure response has been recognized as an effective measure of globally-integrated thermal forcing [*Zurek*, 1981; *Lewis and Barker*, 2005]. This motivates our investigation of the relationship between thermal forcing and the semi-diurnal temperature response. For this purpose, we consider a depth weighted measure of temperature broadly centered at roughly 50-30 Pa. We refer to this as T_{15}, which presents the brightness temperature in the CO_2 15 μm band. This measure has the advantage of emphasizing the relatively barotropic S_2 response (Figure 4e) while smoothing out the contribution from S_1, as described in *Wilson and Richardson* [2000]. The seasonal variation of equatorial $S_2(T_{15})$ for two LMD simulations with and without radiatively active clouds is shown in Figure 5. The dust-only simulation shows the response to the two regional dust lifting events in MY26, with the post-solstice event being particularly prominent. A similar result was shown in *Wilson et al*. [2008] using results from the TES Reanalysis project. The striking aspect of Figure 5 is the relatively large amplitude response to cloud heating throughout the year. This result suggests that cloud heating may dominate dust heating for a significant part of the Mars year and this would be a significant realignment of our understanding of aerosol forcing of the atmosphere if verified by observation.

Since September 2010, MCS has been combining cross-track and along-track views to yield temperature observations at six unequally spaced local times [*Kleinböhl et al.* 2013]. Preliminary analysis suggests the presence of a semi-diurnal temperature signal that is consistent with significant cloud radiative forcing. These results will be presented at the workshop.

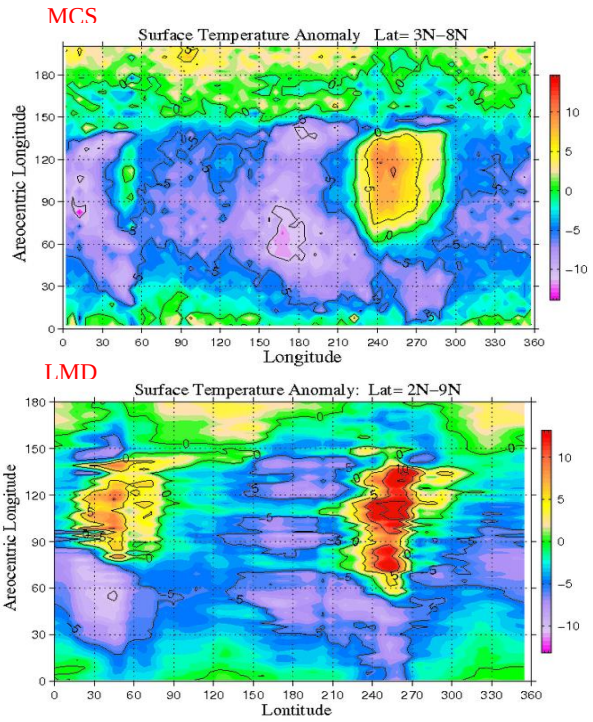

Figure 6. (a) Seasonal evolution of MCS morning (0300 LT) anomaly T_{32} brightness temperature in the 3-8°N latitude band. The anomaly is the departure of the temperature from the annual mean for each longitude. (b) Corresponding anomaly surface temperature variation from the LMD simulation (MCD V5.1).

As described in *Wilson et al*. [2007], the radiative influence of clouds can also be asssessed by the effect of downward IR radiation on nighttime surface temperatures, thus providing an indirect measure of cloud optical depth. Figure 6a shows the seasonal variation of the 3am tropical T_{32} anomaly field, defined as the deviation from the annual mean as a function of longitude. (The 32 μm brightness temperature is a close approximation of true surface temperature [*Wilson et al*. 2011]). The longitude zones associated with Arabia and Tharsis show warm anomalies that have been previously interpreted as the result of enhanced downward IR radiation from

water ice clouds [*Wilson et al*., 2007]. GFDL MGCM simulations suggest that clouds with visible opacities of ~1 contribute sufficient additional IR flux (~15 W/m^2) at the surface to account for the observed surface temperature increase at solstice. Figure 6b shows the temperature enhancement in the LMD simulation. Of course, the downward IR flux will depend on cloud opacity and size distribution, while the surface temperature response is also a function of the underlying surface thermal inertia. We will present results from a number of simulations based on several models to examine the relationships between cloud effective radius, cloud opacity, downward IR flux and surface temperature response.

Summary:

There is ample evidence that radiatively active water ice clouds have a significant impact on the Martian atmosphere. We consider results from an ensemble of simulations to assess robustness and to investigate model biases. We have identified the tropical semi-diurnal tide as a likely significant metric for quantifying cloud radiative forcing. We anticipate that the representation of cloud microphysics, as it controls nucleation and cloud particle size, will emerge as a critical element for accurate simulation. This will be particularly important for assessing the role of dust-cloud interactions that contribute to the aphelion season dust distribution. We anticipate that a broad range of ice particle sizes will need to be accounted for in parameterizations, with smaller particles to allow for the observed deep vertical extent of the tropical cloud layer [*Heavens et al.* 2010] and larger particles to account for the more localized and evidently strong near-surface cooling in the Tharsis and Arabia regions [*Wilson and Guzewich*, submitted paper]. We expect that careful comparison with MCS data will provide valuable guidance and constraints for further model development, particularly for the treatment of cloud microphysics and radiation.

References:

Greybush, S. J., et al. (2012), Ensemble Kalman filter data assimilation of thermal emission spectrometer profiles into a Mars global circulation model. *J. Geophys. Res. Planets*, *117*, E11008, doi:10.1029/2012JE004097.

Guzewich, S.D., E.R. Talaat, A.D. Toigo, D.W. Waugh, and T. McConnochie (2013), High altitude dust layers on Mars: Observations with the Thermal Emission Spectrometer, *J. Geophys. Res.*, *118*, doi: 10.1002/jgre.20076.

Haberle, R.M. et al. 2011 Radiative effects of water ice clouds on the martian seasonal water cycle, *Fourth International workshop on the Mars Atmosphere: Modeling and Observations*, Paris, France

Heavens, N.G., et al. (2010), Water ice clouds over the Martian tropics during northern summer, *Geophys. Res. Lett*., *37*, L18202, doi:10.1029/2010GL044610.

Heavens, N.G., et al. (2011), The vertical distribution of dust in the martian atmosphere during northern spring and summer: Observations by the Mars Climate Sounder and analysis of zonal average vertical dust profiles, *J. Geophys. Res. 116*, E04003, doi:10.1029/2010JE003691.

Hinson, D., and R.J. Wilson (2004), Temperature inversions, thermal tides, and water ice clouds in the martian tropics, *J. Geophys. Res.*, *109*, E01002, doi:10.1029/JE002129.

Kahre, M.A., et al. (2013), Coupling the Mars dust and water cycles: Investigating the role of clouds in controlling the vertical distribution of dust during NH summer, *this workshop*.

Kleinböhl, A., R.J. Wilson, D. Kass, J.T. Schofield, and D.J. McCleese (2013), The semidiurnal tide in the middle atmosphere of Mars, *Geophys. Res. Lett.*, *40*, doi:10.1002/grl.50497.

Lee, C., et al. (2009), Thermal tides in the Martian middle atmosphere as seen by the Mars Climate Sounder. *J. Geophys. Res.*,*114*,E03005, doi:10.1029/2008JE003285.

Lewis, S.R., and P.R. Barker (2005), Atmospheric tides in a Mars general circulation model with data assimilation, *Adv. Space Res. 36*(11), 2162-2168.

Madeleine, J.-B., F. Forget, E. Millour, T. Navarro, and A. Spiga (2012), The influence of radiatively active water ice clouds on the Martian climate, *Geophys. Res. Lett.*, *39*, L23202, doi10.1092/2012GL053564.

Millour, E., et al. (2014), A new Mars climate database, version 5.1, *this workshop*.

Pottier, A., et al. (2014), Improving water ice cloud modeling in the LMD global climate model: Mars Climate Sounder data comparisons, *this workshop*.

Steele, L.J., S.R. Lewis, M.R. Patel, L. Montabone, and F. Forget (2014), The radiative impact of water ice clouds from assimilation of Mars Climate Sounder data, *this workshop*.

Wilson, R.J., and M.I. Richardson (2000), The Martian atmosphere during the Viking mission, 1: Infrared measurements of atmospheric temperatures revisited. *Icarus,* 145, 555-579.

Wilson, R.J., G. Neumann, and M.D. Smith (2007), The diurnal variation and radiative influence of martian water ice clouds, *Geophys. Res. Lett*., 34, L02710, doi:10.1029/2006GL027976.

Wilson, R. J., S. R. Lewis, L. Montabone, and M. D. Smith (2008), Influence of water ice clouds on Martian tropical atmospheric temperatures, *Geophys. Res. Lett.*, 35, L07202, doi:10.1029/2007GL032405.

Wilson, R.J., J. Noble, and S.J. Greybush (2011), The derivation of atmospheric opacity from surface temperature observations, *Fourth International workshop on the Mars atmosphere: modeling and observations*, Paris, France.

Wilson, R.J. (2011), Water ice clouds and thermal structure in the martian tropics as revealed by Mars Climate Sounder, *Fourth International workshop on the Mars atmosphere: modeling and observations*, Paris, France.

Wilson, R.J. (2011b), Dust cycle modeling with the GFDL Mars general circulation model, *Fourth International workshop on the Mars atmosphere: modeling and observations*, Paris, France.

Wilson, R.J., and S.D. Guzewich (2013), Influence of water ice clouds on nighttime tropical temperature structure as seen by the Mars Climate Sounder, submitted to *Geophys. Res. Lett*.

Zurek, R.W. (1981), Inference of dust opacities for the 1977 Martian great dust storms from Viking Lander 1 pressure data, *Icarus*, *45*, 652-670.